

# OpenSU3D: Open World 3D Scene Understanding using Foundation Models

Rafay Mohiuddin<sup>\*,1</sup>, Sai Manoj Prakhya<sup>2</sup>, Fiona Collins<sup>1</sup>, Ziyuan Liu<sup>2</sup> and André Borrmann<sup>1</sup>

**Abstract**—In this paper, we present a novel, scalable approach for constructing open set, instance-level 3D scene representations, advancing open world understanding of 3D environments. Existing methods require pre-constructed 3D scenes and face scalability issues due to per-point feature vector learning, limiting their efficacy with complex queries. Our method overcomes these limitations by incrementally building instance-level 3D scene representations using 2D foundation models, efficiently aggregating instance-level details such as masks, feature vectors, names, and captions. We introduce fusion schemes for feature vectors to enhance their contextual knowledge and performance on complex queries. Additionally, we explore large language models for robust automatic annotation and spatial reasoning tasks. We evaluate our proposed approach on multiple scenes from ScanNet [1] and Replica [2] datasets demonstrating zero-shot generalization capabilities, exceeding current state-of-the-art methods in open world 3D scene understanding. Project page: <https://opensu3d.github.io/>

## I. INTRODUCTION

### A. Motivation

Recent AI advancements have led to significant breakthroughs in open-set object detection and contextual understanding in 2D images, primarily due to pre-trained foundation models such as CLIP [3], SAM [4] and the integration of vision with language models [5], [6]. However, translating these successes to 3D scenes remains challenging. Current 3D approaches [7]–[11], while innovative, have not yet matched their 2D counterpart’s performance. Bridging this gap is crucial for applications requiring 3D interaction, such as robotics and digital twins, to revolutionize how we perceive and interact with the three-dimensional world.

### B. Limitations of Current Methods

Recent works [7]–[11] have impressively integrated 2D foundation models for open-world 3D scene understanding. However, these methods have several limitations. Most of these methods are designed as batch-processing or non-incremental methods requiring the availability of complete 3D scene data before-hand, which is unrealistic in real world operation of many robotics applications. Primarily, these methods generate 3D feature vectors from 2D foundation models like CLIP [3], [12], but lack a universal strategy for 2D to 3D information extrapolation coming from other types of 2D foundation models. Furthermore, the creation of dense, per-point feature vectors not only poses memory

and scalability issues but also complicates the critical task of isolating distinct entities within a scene, which is essential for practical applications. Most notably, the existing methods seem to work effectively for simple queries but lack the depth and contextual understanding required for more complex spatial queries/tasks.

### C. Proposed Approach

We introduce a novel approach for constructing open-set 3D scene representation that addresses open vocabulary instance recall (object search), segmentation, annotation, and spatial reasoning. Our method leverages 2D foundation models to extract instance-level information from RGB-D images, using GroundedSAM [13] to obtain masks, bounding boxes, names, and prediction scores and GPT-4V [6] for detailed caption. For each instance, feature vectors are extracted from CLIP [3] at multiple scales and fused. Every instance in an image is assigned a unique ID and has an associated 2D segmentation mask. These masks are back-projected using depth and pose data to construct a per-image segmented 3D scene. Our approach tracks and updates the 2D and 3D segmentation masks and corresponding meta-information based on overlapping region based techniques, enabling efficient, scalable, and incremental 3D scene construction as the environment is explored. The instance-level representation and feature fusion schemes incorporate local context, aiding in distinguishing instances within the same class in relational queries.

### D. Key contributions

This study brings the following key contributions to the field of 3D scene understanding:

1. We introduce an incremental and scalable approach for open-set 3D scene understanding and instance segmentation that seamlessly integrates instance-level information from individual images, utilizing 2D foundational models, into a unified 3D scene representation.
2. We develop an innovative feature fusion formulation that enables the identification of instances within the same class through contextual queries and improves the overall open vocabulary 3D object search performance.
3. We explore the use of large language models in conjunction with our constructed 3D scene representations for automatic annotation and complex spatial reasoning queries.

## II. RELATED WORK

### A. Foundation & Large Language Models

Foundation models, trained on large scale data, have revolutionized AI by achieving unprecedented performance

\* Corresponding author rafay.mohiuddin@tum.de

<sup>1</sup> Chair of Computational Modeling & Simulation, Technical University of Munich, 80333 Arcisstraße 21, Germany

<sup>2</sup> Intelligent Cloud Technologies Lab, Huawei Munich Research Center, 80992 Riesstraße 25, Germany

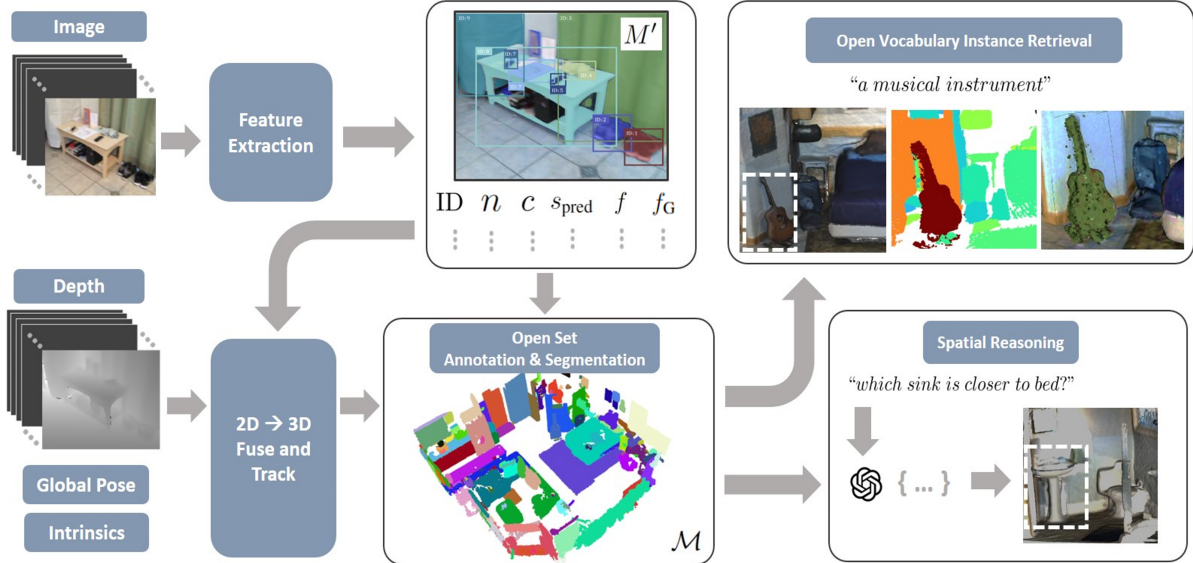


Fig. 1: **Open World 3D Scene Understanding Pipeline.** Our method takes a sequence of RGB-D images and constructs a 3D scene representation for open vocabulary instance retrieval, open set annotation, segmentation, and spatial reasoning.

across diverse tasks. CLIP [3], BLIP [14], and similar models integrate visual and textual data to create unified representations, enabling improved performance in multimodal tasks such as image captioning, visual question answering, and cross-modal retrieval. In segmentation, LSeg [15], and OVSeg [16] offer promptable and open-vocabulary capabilities. Grounded models like GSAM [13] and SEEM [17], building on top of SAM [4], contextualize outputs by incorporating additional semantic and situational information, thereby enhancing the interpretative accuracy and relevance of model predictions. This allows for more precise and context-aware applications in tasks such as image segmentation, object detection, and scene understanding. Language models [18], [19] have excelled in natural language tasks, while their integration with vision [6], [20] advances open-world understanding. This work explores a generalizable approach for extracting and linking information between 2D images and 3D spaces, leveraging the capabilities of foundation and large language models.

### B. 3D Scene Segmentation

Semantic segmentation is a key challenge in 3D vision. Methods like Voxblox++ [21] and Kimera [22] merge semantics with SLAM, while others methods like Hydra [23], Scene Graph Fusion [24]) build 3D scene graph on top of semantically segmented scene, however, these techniques still operate within a closed-set paradigm. Recent works, including [25] and SAM3D [26], identify 3D instances by analyzing overlapping semantically segmented points back-projected from RGB images and generates open-set fine-grained 3D masks non-incrementally. In contrast, [25] offers an incremental, closed-set sparse point map approach with fixed computation per update. We propose an incremental method using SAM’s 2D masks and region overlap-based techniques, generating fine-grained 3D instance masks with

constant update computation. Additionally, our approach efficiently tracks 2D-3D mask IDs, facilitating efficient information transfer from per-image masks to full 3D scene.

### C. 3D Scene Understanding

3D scene understanding has evolved significantly by leveraging 2D vision-language models, mapping their rich features onto 3D spaces for open vocabulary queries. Initial works like OpenScene [8] and ConceptFusion [11] project 2D feature vectors from CLIPSeg [12] and CLIP [3] into 3D, demonstrating potential but poses computational and scalability issues due to dense, per-point representations. Recent work OpenMask3D [27] offers an instance-centric approach using Mask3D [28], avoiding scalability issues but it’s still non-incremental, requiring all the data beforehand. Additionally, some studies [11], [27] explore advanced feature engineering, fusing CLIP vectors from object-centric and larger image sections to capture both local and global context. Despite progress, challenges in computation, scalability, and non-incremental approaches necessitate more efficient, adaptable, and versatile solutions.

### D. 3D Spatial Reasoning

Global 3D spatial reasoning remains challenging in open-world scene understanding scenarios. Recent works 3DCLR [7], 3DLLM [9] and GroundedLLM [29] propose innovative approaches leveraging LLM for 3D reasoning, yet accurate 2D spatial reasoning is still challenging for models like GPT-4V [6], as shown in [30]. For 2D spatial reasoning, recent works like Set of Mark Prompting [30] explores prompting methods to directly use GPT4V [6]. We adapt this approach [30], employing LLMs for 3D spatial reasoning over our constructed scenes via strategic prompting.

### E. Concurrent Work

Concurrently, methods like Segment3D [31], OpenIns3D [32] and SayPlan [33] also tackle 3D scene understanding. OVSG [16] and ConceptGraph [34] closely align with our focus on incremental, scalable instance-based representation. However, we uniquely rely on geometric principles for merging 3D masks, and not CLIP similarity, resulting in better performance as shown in experiments. Additionally, instead of constructing separate scene graphs for spatial reasoning; we instead tap LLM’s innate reasoning abilities via tailored prompts over our constructed scene.

## III. METHOD

Our method, processes a sequence of RGB-D images along with their poses to create an open set 3D scene representation for open world scene understanding tasks like, open vocabulary object retrieval, 3D segmentation, annotation and spatial reasoning. Illustrated in Fig. 1 the pipeline contains two main modules:

**1. Per-Image Feature Extraction:** Extracts instance-level masks, embeddings, and meta-information from each image and assigns a unique ID to each instance for precise tracking.

**2. 2D to 3D Fusion and Tracking:** Creates a 3D semantic map from per-image 2D masks and associates 2D information into 3D space by tracking the corresponding IDs.

### A. Per-Image Feature Extraction

The feature extraction process, as shown in Fig. 2, begins with a sequence of RGB images,  $\mathcal{I} = \{I_0, I_1, I_2, \dots, I_n\}$ . A subset  $\mathcal{I}' = \{I_0, I_s, I_{2s}, \dots, I_n\}$  is sampled with a stride  $s$  which ensures a reasonable overlap to minimize computational redundancy. For each image  $I' \in \mathcal{I}'$ , groundedSAM [13] is used to obtain 2D masks  $M$ , bounding boxes  $BB$ , and prediction scores  $S_{\text{pred}}$ . Crops of each instance, based on  $bb \in BB$ , are passed to GPT-4V [6] to get labels (names)  $N$  and detailed captions  $C$  describing the object.

Each instance is assigned a unique ID, and masks  $M$  are updated to  $M'$  with these IDs and by adding a border of  $px$  pixels around each mask to delineate entities. Feature vectors are extracted using the CLIP encoder in two stages:

- 1) A global feature vector  $f_G$  is extracted for full image.
- 2) Instance-specific feature vectors  $F = \{f_{MS}\}$  are created by first cropping the image at multiple scales based on scaling ratios  $S_r = \{s_r\}_k$  and then fusing per-crop vectors  $\{f\}_k$  with a multi-scale feature fusion scheme as discussed in Sec III-D.

The updated masks  $M'$ , and instance-level metadata including IDs, names  $n \in N$ , captions  $c \in C$ , prediction scores  $s_{\text{pred}} \in S_{\text{pred}}$ , fused feature vectors  $f_{MS} \in F$ , and global feature vector  $f_G$ , are stored for each image in  $\mathcal{I}'$ .

### B. 2D to 3D Fusion & Tracking

As shown in Fig. 3, we initiate the fusion and tracking module by initializing an empty 3D point cloud for the complete 3D scene, represented as  $\mathcal{P}_{\text{scene}} \in \mathbb{R}^{x,y,z,\text{ID}}$ , and a global hash table  $\mathcal{Q}$  for tracking the unique IDs, defined as:  $\mathcal{Q} : \mathcal{Q} \mapsto \{\text{ID} \in \text{uniq}(\text{ID} \in \mathcal{P}_{\text{scene}}) : \{\text{ID} \in \{M'\}\}\}$

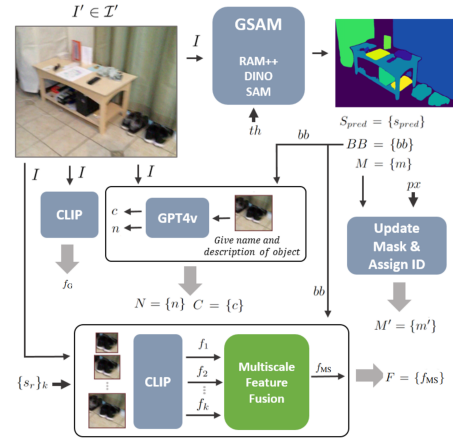


Fig. 2: **Feature extraction:** Using Grounded-SAM, we extract masks and labels for each image. The labels are further refined and mask description is obtained using GPT-4V. Lastly, a global per-image CLIP feature and fused multi-scale per-mask CLIP features are extracted and stored.

For the image  $I'$ , associated elements including depth maps  $D$ , global poses  $T$ , updated masks  $M'$ , and camera intrinsic  $K$  are retrieved. Each pixel  $(u, v) \in I'$  is back-projected into 3D space, using depth data and is assigned a semantic label corresponding to the mask  $M'$ , resulting in a 3D point cloud for a single image  $\mathcal{P}_{\text{frame}}$ .

$$\mathcal{P}_{\text{frame}} = \left\{ \left( T \cdot \left( D(u, v) \cdot K^{-1} \cdot \begin{pmatrix} u \\ v \\ 1 \end{pmatrix} \right), M'(u, v) \right) \right\} \quad (1)$$

Using the bounds of  $\mathcal{P}_{\text{frame}}$ , we sample  $\mathcal{P}'_{\text{scene}}$  from  $\mathcal{P}_{\text{scene}}$ , containing only points within the bounds of  $\mathcal{P}_{\text{frame}}$ . A  $KDTree$  search is performed, utilizing Euclidean distance function,  $d(\cdot, \cdot)$  to matches points  $\mathbf{p} \in \mathcal{P}_{\text{frame}}$  with points  $\mathbf{q} \in \mathcal{P}'_{\text{scene}}$ . If  $d(\mathbf{p}, \mathbf{q}) < \epsilon$ , we group the indices corresponding to  $\mathbf{p} \in \mathcal{P}_{\text{frame}}$  with  $\mathbf{q} \in \mathcal{P}_{\text{scene}}$  to obtain the respective index pairs  $\{(\mathbf{i}_{\text{frame}}, \mathbf{i}_{\text{scene}})\}$  for all overlapping points. This search strategy limits the search space of  $KDTree$  to only overlapping region, thereby requiring a constant computation (search space) per update.

To track and update matched IDs, similar to SAM3D’s [26] approach, we begin by obtaining a list of unique IDs  $\{\text{ID}_f\}$  for each segment and a corresponding list denoting the total point count  $\{c_{\mathcal{P}_f}\}$  of each segment of  $\mathcal{P}_{\text{frame}}$ .

For each segment in  $\mathcal{P}_{\text{frame}}$  with  $c_{\mathcal{P}_f} \in \{c_{\mathcal{P}_f}\}$ , we utilize the index pairs  $\{(\mathbf{i}_{\text{frame}}, \mathbf{i}_{\text{scene}})\}$  to obtain the set of points from  $\mathcal{P}_{\text{scene}}$  that overlaps with  $\mathcal{P}_{\text{frame}}$ . From these points, we derive a list of unique segment IDs  $\{\text{ID}_s\}$  and their corresponding total point counts  $\{c_{\mathcal{P}_s}\}$ .

$$\text{OverlapRatio} = \frac{\max(\{c_{\mathcal{P}_s}\})}{\min(c_{\mathcal{P}_f}, \max(\{c_{\mathcal{P}_s}\}))} \quad (2)$$

If the overlap ratio satisfies a pre-defined threshold, i.e.,  $\text{OverlapRatio} \geq \rho$ , we perform an ID replacement and update operation. Specifically, all  $\text{ID}_f \in c_{\mathcal{P}_f}$  present in the  $\mathcal{P}_{\text{frame}}$

are replaced with  $ID_s \in \max(\{c_{\mathcal{P}_s}\})$  to get,  $\mathcal{P}'_{\text{frame}}$  which is then concatenated to  $\mathcal{P}_{\text{scene}}$ . Additionally, set of points from  $\mathcal{P}'_{\text{scene}}$  can also be deleted to retain constant sparsity, ensuring fixed computation requirement per update.

The updated IDs are then appended to the  $\mathcal{Q}$ , conversely, if the overlap ratio does not meet the threshold requirement, a new entry is added in  $\mathcal{Q}$ .

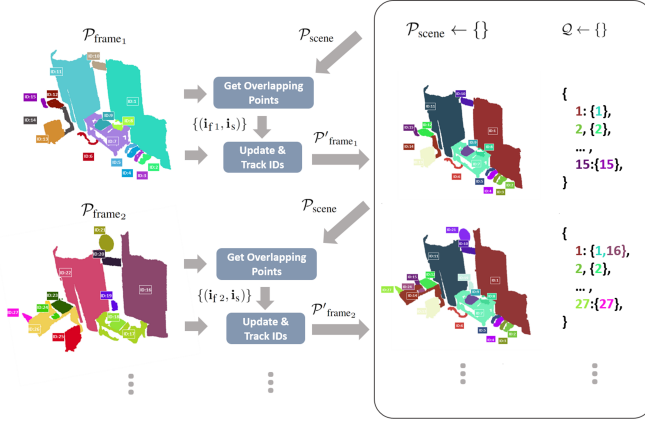


Fig. 3: **2D-3D Fusion and Tracking:** It tracks and updates IDs of each back-projected semantic mask associated with an image by efficiently assessing the overlap region with other semantic masks. Essentially, the tracked IDs are recorded and updated mask-projections are concatenated.

### C. Post Processing

The updated point cloud  $\mathcal{P}_{\text{scene}}$  with updated corresponding IDs based on overlap ratio in  $\mathcal{Q}$ , along with per-image meta data is processed to construct an instance-centered 3D map of the processed whole scene  $\mathcal{M}$ , defined as:

$$\mathcal{M} = \{(\mathcal{P}, n, c, f_{MV}, bb_{3D}, (x_c, y_c))_i | i \in \text{uniq}(\text{ID} \in \mathcal{P}_{\text{scene}})\} \quad (3)$$

For each distinct 3D object  $\mathcal{P}_i$ , we perform DBSCAN based clustering to reduce noise and achieve fine-grained segmentation. Accordingly, 3D bounding boxes  $bb_{3D,i}$  and their centroids  $(x_c, y_c)_i$  are recomputed. For each multi-view image corresponding to the 3D object  $\mathcal{P}_i$ , the 2D IDs  $\mathcal{Q}[\text{ID} \in \mathcal{P}_i]$ , names  $N'$ , captions  $C'$ , prediction scores  $S'_{\text{pred}}$ , and feature vectors  $F'$  are retrieved using  $\mathcal{Q}$  for aggregation and fusion. The label  $n_i$  and caption  $c_i$  of each 3D instance  $\mathcal{P}_i$  are assigned using the maximum prediction score  $S'_{\text{pred}}$ , alternatively the labels for each object-crops in images with top  $m$  prediction scores  $S'_{\text{pred}}$  are refined using a LLM [6] with prompt: “assign a name to the object based on a given list of names”, yielding more accurate names  $n'_i$ . Lastly, features vectors corresponding to multiple views  $f_{MV}$  are obtained via multiview scheme as described in Sec. III-D by fusing feature vectors with top  $m$  scores  $S'_{\text{pred}}$ .

### D. Feature Fusion

Given a list of feature vectors  $\{f\}_k$  from multiple scale crops of an instance in an image and feature vectors  $\{f_{MS}\}_m$

corresponding to multiple view of images of a 3D instance, a simple and direct fusion scheme aggregates these feature vectors as shown below:

$$f_{MS} = \frac{1}{k} \sum_{i=1}^k f_i \quad (4) \quad f_{MV} = \frac{1}{m} \sum_{i=1}^m f_{MS_i} \quad (5)$$

However, this simple fusion schemes described in Eq. 4 and Eq. 5 is limited and offers lower performance on relative queries as highlighted later in ablation studies in Sec. V-A. Moreover, as also highlighted in findings from OpenMask3D [27], it was observed that multiscale crops add redundant context, with larger crops deteriorating overall object recall performance. To address these issues, we propose a modified multi-scale fusion scheme as shown in Eq. 6. Our proposed fusion scheme effectively down weighs the influence of larger crops by assigning weights based on cosine similarity to the best-fit crop.

$$f_{MS} = \frac{1}{k} \sum_{i=1}^k \left( \frac{f_1 \cdot f_i}{\max(\|f_1\|_2 \cdot \|f_i\|_2)} \right) \cdot f_i \quad (6)$$

For the integration of multiview features, we draw parallels to the approach in ConceptFusion [11] which focuses on the fusion of 2D per-pixel features, we propose the direct incorporation of a global feature vector  $f^g$ , while synthesizing multiview feature vectors for each instance, defined as:

$$f_{MV} = \frac{1}{m} \sum_{i=1}^m \left( f_{MS_i} + \left( \frac{f_{MS_i} \cdot f_{G_i}}{\max(\|f_{MS_i}\|_2 \cdot \|f_{G_i}\|_2)} \right) \cdot f_{G_i} \right) \quad (7)$$

### E. Instance Retrieval & Segmentation

Given a map  $\mathcal{M}$ , open vocabulary 3D object search or 3D instance retrieval and segmentation operates in two stages. First, a query  $\mathcal{K}$  is processed using the CLIP text encoder to obtain the feature vector  $f_{\mathcal{K}}$ . Second, a cosine similarity score is computed for all 3D instances  $\{S_{\text{score}}\}$ , and the segmentation mask of the 3D instance with maximum similarity score,  $\mathcal{M}[\text{argmax}(\{S_{\text{score}}\})]$  is retrieved as the most likely response to the query  $\mathcal{K}$ .

### F. Spatial Reasoning

For queries involving complex spatial reasoning, the key idea is to leverage the long context window of Large Language Models like GPT-4 [6], to perform spatial reasoning based on coherent 3D representation and meta data such as mask labels, centroids, bounding boxes and description available for the constructed scene  $\mathcal{M}$ , using in-context learning. A simplified map  $\mathcal{M}' := \mathcal{M} \setminus \{\mathcal{P}, f_{MV}\}$  is passed along with system prompt designed using the prompting strategy defined as:

- Use ‘Name’ & ‘Description’ to understand object.
- Use ‘ID’ to refer object.
- Use ‘Cartesian Coordinates’.
- Get ‘Centroid’ & ‘Bounding Box’ information.
- Compute ‘Euclidean Distance’ if necessary.
- Assume ‘Tolerance’ if necessary.

## IV. EXPERIMENT SETUP

### A. Datasets

Multiple scenes from the semi-synthetic dataset Replica [2] (*room0*, *room1*, *room2*, *office0*, *office1*, *office2*, *office3*, *office4*) and real-world ScanNet [1] (*scene0000\_00*, *scene0034\_00*, *scene0164\_03*, *scene0525\_01*, *scene0549\_00*) were used for thorough qualitative and quantitative evaluation. Similar to previous studies [11], [34], a limited number of scenes were selected due to the extensive manual human evaluation.

### B. Implementation Details

1) *Models Utilized*: GroundedSAM [13] (a method based on RAM++ [35] (*ram\_plus\_swin\_large\_14m*), GroundingDINO [36] (*groundingdino\_swin\_tgc*), and SAM [4] (*sam\_vit\_h\_4b8939*)) is employed for generating instance segmentation masks and bounding boxes. GPT-4V [6] (*gpt-4-vision-preview*, *gpt-4-1106-preview*) is used to create detailed captions & names for the instances and spatial reasoning. The CLIP encoder [3] (ViT-H-14 pre-trained on *laion2b\_s32b\_b79k* dataset) is used for instance feature vectors.

2) *Hyper parameter Settings*: Same hyper parameters are used across datasets, determined by ablation studies on Replica [2] (Sec: V-A). We set  $m = 5$ , selecting top 5 images and apply  $k = 3$ , using 3 level of crops with a 0.2 increment in scaling ratio i.e  $S_r = [0.8, 1, 1.2]$ . A stride of  $s = 40$  is used to ensure adequate overlap between frames in chosen datasets. For GroundedSAM [13], thresholds are set as follows: IoU-0.4, bounding box-0.25, and text-0.25. A padding of  $px = 20$  pixels delineates borders between instance masks. Overlap ratio evaluation uses a voxel size of  $\epsilon = 0.02$  and an overlap threshold of  $\rho = 0.3$ . DBSCAN post-processing employs an epsilon of 0.1 and a minimum cluster size of 20 points. GPT-4 [6] is configured with a temperature of 0.

3) *Filtering and Post-Processing*: Large background objects (walls, ground, roof, ceiling) and objects with bounding boxes  $> 95\%$  of image area are excluded to prevent their feature vectors from exhibiting similarity to foreground objects, adversely affecting recall and score distribution. In DBSCAN post-processing, clusters with points  $\geq 80\%$  of the largest cluster are treated as separate instances with unique IDs and attributes. In cases where an object is undetectable by GPT-4 [6], instances are assigned RAM++ [35] names and given simplified captions: "an object in a scene".

### C. Quantitative Evaluation

The proposed method is evaluated using standard metrics: mean recall accuracy (mAcc), frequency-weighted IoU (F-mIoU), and average precision (AP) at IoU thresholds [0.5:0.05:0.95], along with AP50 and AP25 as defined in ScanNet [1]. For open vocabulary performance, similar to [27], [34], we retrieved 3D masks using ground truth labels with the prompt 'an object in a scene'. We downsample retrieved and ground truth masks to 0.25cm voxel size and applied a nearest neighbor search for intersecting points

identification. We compared our results on the Replica [2] dataset with state-of-the-art models [11], [27], [31], [34], using identical prompts and foundation models.

### D. Qualitative Evaluation

Extensive qualitative assessment for open vocabulary instance retrieval, annotation, segmentation, and spatial reasoning was performed with manual human evaluation. For **open vocabulary instance retrieval**, over 1,000 queries regarding instances, affordances, properties, and relative queries were made. Performance was evaluated using CLIP [3] and four fusion schemes: *Scheme 1* represents direct aggregation of multiscale (Eq. 4) and multiview features (Eq. 5), *Scheme 2* represents updated multi-view features (Eq. 7), *Scheme 3* represents updated multi-scale features (Eq. 6) with increased crop expansion ratios ( $S_r = [1, 2, 4]$ ), and *Scheme 4* represents combination of updated multi-view (Eq. 7) and multi-scale (Eq. 6) features fusion formulation.

The **Annotation and Segmentation** capabilities of the proposed approach were evaluated through manual verification of label assignments and mask merging. For **spatial reasoning**, 70 complex questions were administered across all scenes using a large language model (see Section III-F), assessing prompting strategy's viability for spatial reasoning.

## V. RESULTS AND DISCUSSION

### A. Ablation Studies

To assess the influence of hyperparameters, ablation studies were conducted on Crop Level  $k$ , Top Images  $m$ , and Crop Ratios  $S_r$  using quantitative metrics. Top Images  $m$  affects multiview feature fusion (Eq. 7), representing the feature vectors for aggregation. Crop Ratio  $S_r$  and Crop Level  $k$  affect multi-scale feature fusion (Eq. 4), determining crop size and quantity for feature vector aggregation. Crop Level  $k$  amplifies Crop Ratio  $S_r$ 's effect, as a higher  $k$  with the same  $S_r$  results in larger crops.

Similar to OpenMask3D [27], we found that extreme values of these hyperparameters deteriorate results. A low  $m$  reduces redundancy, while a high  $m$  may include bad images, as shown in Table I. Lower values of  $S_r$  and  $k$  may not harm the model but could introduce redundancy. Larger  $S_r$  values add context but may saturate similarity scores.

Parameter	Value	Replica [2]				
		mAcc	F-mIoU	AP	AP50	AP25
Top Images ( $m$ )	1.0	39.6	43.4	8.7	19.3	27.2
	5.0	<b>40.8</b>	<b>44.7</b>	<b>8.9</b>	<b>19.6</b>	<b>27.7</b>
	10.0	39.3	44.3	8.7	19.1	27.5
Crop Levels ( $k$ )	1.0	35.9	43.6	<b>9.1</b>	<b>19.6</b>	<b>27.7</b>
	3.0	<b>40.8</b>	<b>44.7</b>	8.9	<b>19.6</b>	<b>27.7</b>
	5.0	39.4	44.3	8.8	19.4	26.9
Crop Ratio ( $S_r$ )	[0.1,1,1.1]	39.9	44.4	<b>8.9</b>	19.4	<b>28.1</b>
	[0.8,1,1.2]	<b>40.8</b>	<b>44.7</b>	<b>8.9</b>	<b>19.6</b>	27.7
	[0.7,1,1.3]	39.9	44.8	<b>8.9</b>	19.4	27.3

TABLE I: **Ablation study of Hyperparameters.** The total images  $m$  w.r.t best prediction scores ( $s_{pred}$ ), for multiview feature fusion. Increment in ratio  $S_r$  for scaling crop sides and total number of crops  $k$ , for multiscale feature fusion.

Additionally, an ablation study with different CLIP model variants was also conducted. As shown in Table II, larger CLIP variants improved overall performance. As an example, Fig. 4 illustrates that a larger CLIP model better associates properties with the queried object, distinguishing between “single sofa” and “double sofa”.

CLIP Models	Replica [2]				
	mAcc	F-mIoU	AP	AP50	AP25
ViT-L-14	38.9	40.2	9.3	20.5	30.3
ViT-H-14	<b>42.6</b>	<b>40.9</b>	<b>9.9</b>	<b>21.6</b>	<b>31.6</b>

TABLE II: **Ablation study of CLIP models.** Influence of different CLIP Models on instance recall performance.

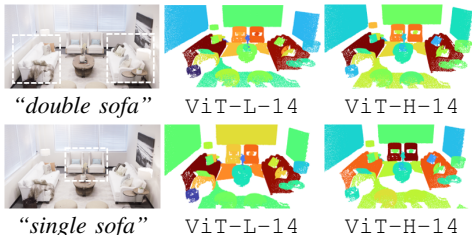


Fig. 4: **Text-Instance Similarity Heatmaps.** For a text query, per-instance cosine similarity heatmaps for different CLIP models. ■: max, ■: min similarity.

### B. Open Vocabulary Instance Retrieval

#### 1) Quantitative Comparison with Baseline Methods:

The proposed method demonstrates comparable or better performance than baselines on quantitative metrics, as shown in Tables III and IV. These compare segmentation mask accuracy and precision in response to open vocabulary queries against ground truth masks. We followed the original ConceptGraph [34] and OpenMask3D [27] setups for fair comparison. Overall, our method performed on par or better across all metrics and datasets.

Method	Replica [2]	
	mAcc	F-mIoU
ConceptFusion [11]	24.2	31.3
ConceptFusion+SAM [11]	31.5	38.7
ConceptGraph [34]	40.6	36.0
ConceptGraph-Detector [34]	38.7	35.4
OpenSU3D (Ours)	<b>42.6</b>	<b>40.9</b>

TABLE III: **Comparison of open-vocabulary segmentation results** with ConceptGraph [34] setup.

Method	Replica [2]		
	AP	AP50	AP25
OpenMask3D [27]	<b>13.0</b>	18.4	24.2
OpenMask3D+Segment3D [31]	-	18.7	-
OpenSU3D (Ours)	8.9	<b>19.6</b>	<b>27.7</b>

TABLE IV: **Comparison of open-vocabulary segmentation results** with OpenMask3D [27] setup.

2) *Qualitative Comparison with Baseline Methods:* The quantitative evaluation was primarily designed for closed vocabulary assessments, relying on recall accuracy that does not reflect real-world requirements for open vocabulary queries. These methods, dependent on the quantity of mask proposals [31], may not accurately represent true performance.

To address these limitations, we provide comprehensive qualitative comparisons with baseline works in Fig. 5. The goal is to assess the ability to recall the correct segmentation mask for open vocabulary queries, assigning high similarity scores to relevant objects and lower scores to irrelevant ones. Specifically, our proposed method showed better 2D to 3D association and distribution of similarity scores with proposed multi-scale and multi-view feature fusion formulation (Eq. 6 and Eq. 7). As shown in Fig. 5, for the queries “a picture on wall” and “an empty vase”, both baseline methods recalled incorrect objects, while our method works perfectly.

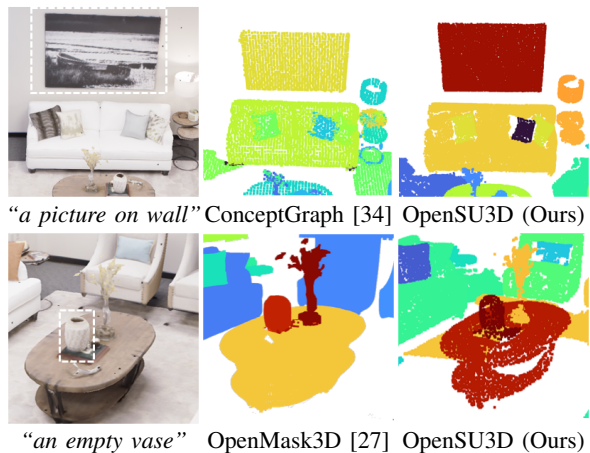


Fig. 5: **Text-Instance Similarity Heatmaps.** Cosine similarity for text queries using ConceptGraph [34], OpenMask3D [32] and our method. ■: max, ■: min similarity.

3) *Assessment of Feature Fusion Schemes:* We conducted a qualitative evaluation of feature fusion schemes as defined in Sec. IV-D. The results are summarized in Table V.

For *Instance*, *Property*, and *Affordance* queries, performance across all schemes was similar. However, for *Relative* queries, *Scheme 2* and *Scheme 3* with our proposed multi-scale and multi-view fusion formulations (Eqs. 7 and 6) outperformed *Scheme 1*. *Scheme 4*, incorporating both the proposed formulations, achieved the best recall accuracy for segmentation masks.

Similarity score heatmaps as shown in Fig. 7 show that *Scheme 1* often wrongly assigned the highest score to the largest instance. In contrast, the updated fusion formulations in *Schemes 2, 3, and 4* improved the recall of instance masks and similarity score distribution, with *Scheme 4* performing the best overall.



Fig. 6: **Text-Instance Similarity per Query Type.** cosine similarity score of each instance for different query types. ■: max, ■: min similarity.

Feature Fusion	Replica [2]				ScanNet [1]			
	Inst.	Aff.	Prop.	Rel.	Inst.	Aff.	Prop.	Rel.
Scheme 1	0.8	0.7	0.7	0.3	0.8	<b>0.8</b>	0.7	0.4
Scheme 2	0.8	0.7	<b>0.9</b>	0.5	<b>0.9</b>	0.7	<b>0.8</b>	0.6
Scheme 3	<b>0.9</b>	<b>0.9</b>	<b>0.9</b>	<b>0.6</b>	<b>0.9</b>	<b>0.8</b>	0.7	0.6
Scheme 4	0.8	<b>0.9</b>	<b>0.9</b>	<b>0.6</b>	<b>0.9</b>	0.7	0.7	<b>0.7</b>

TABLE V: **Evaluation of feature fusion schemes.** Accuracy of fusion schemes for retrieval with “Inst.” (instance), “Aff.” (affordance), “Prop.” (property), and “Rel.” (relative) text queries, as assessed by a human evaluator.

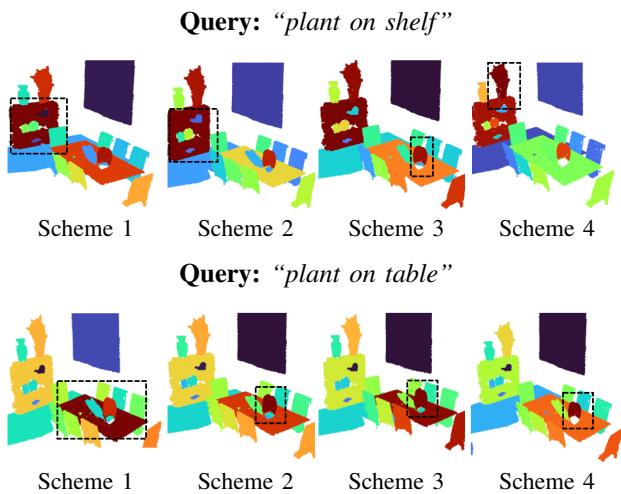


Fig. 7: **Relative Query Similarity Heatmaps.** For a given text query, per-instance cosine similarity heatmaps across feature fusion schemes. ■: max, ■: min similarity.

### C. Open Set Annotation and Segmentation

Annotation accuracy for directly assigned label  $n$  with maximum prediction score  $S'_{\text{pred}}$  and LLM refined top  $m$  labels corresponding to  $S'_{\text{pred}}$  label  $n'$  (discussed in III-C), were manually verified across all Replica [2] and ScanNet [1] scenes. To evaluate open set segmentation, under-merges and over-merges were counted and classified as faulty. Corresponding experiments in Table VI indicates that LLM labels  $n'$  are more accurate than direct labels  $n$ , highlighting that redundancy improves label (name) assignment while

filtering undesired instances (Sec. V-A). This leads to a slight improvement in mask merging accuracy. Additionally, LLM labels  $n'$  are more concise than direct labels  $n$ .

Labels	Replica [2]		ScanNet [1]	
	Label Acc.	Merge Acc.	Label Acc.	Merge Acc.
Direct Label ( $n$ )	0.83	0.87	0.75	0.85
LLM Label ( $n'$ )	<b>0.87</b>	<b>0.88</b>	<b>0.84</b>	<b>0.87</b>

TABLE VI: **Qualitative evaluation of segmentation and annotation accuracy.** For Direct Label ( $n$ ) and LLM Label ( $n'$ ), the annotation and merge accuracy of segmentation masks, as assessed by a human evaluator.

### D. Complex Spatial Queries

To assess spatial reasoning, we posed 70 complex spatial questions (Example, Fig. 1 “Which sink is closer to bed”) across scenes as specified in Sec. III-F. The manual assessment showed that, with our prompting strategy, LLM demonstrated effective reasoning in 3D space, over constructed representation. LLM exhibited higher accuracy in for scenes from Replica [2] (0.83), compared to ScanNet [1] (0.68). This decline in performance in larger scenes is attributed to a higher incidence of merging flaws and labels associated to larger scenes.

### E. Limitations

The effectiveness of this approach is constrained by the capabilities of its underlying foundation models and the occurrence of merging errors. The method leverages CLIP for image-text association and GroundedSAM for 2D mask generation, making its performance directly tied to the robustness of these foundational models. Furthermore, the method’s spatial reasoning and annotation accuracy depends on LLM [6] and are impacted by occasional merging faults.

## VI. CONCLUSION

In conclusion, this study presents a scalable and incremental framework for open world 3D scene understanding, addressing limitations of current non-incremental methods. By

leveraging 2D foundation models, our approach constructs detailed instance-level 3D scene representations, efficiently tracking and associating instance-specific information such as feature vectors, names, and captions. The proposed feature fusion schemes enhance the model’s ability to contextualize and interpret complex queries. Additionally, the use of large language models for automatic annotation and advanced spatial reasoning tasks demonstrates the method’s versatility and robustness. Comprehensive evaluations show that our method achieves superior zero-shot generalization compared to state-of-the-art solutions. In future, we plan to explore spatio-temporal reasoning in 3D dynamic scenes and extend the method from indoors to large-scale outdoor environments.

## REFERENCES

- [1] A. Dai, A. X. Chang, M. Savva, M. Halber, T. Funkhouser, and M. Niessner, “Scannet: Richly-annotated 3d reconstructions of indoor scenes,” in *2017 IEEE Conference on Computer Vision and Pattern Recognition (CVPR)*, July 2017.
- [2] J. Straub, T. Whelan, L. Ma, Y. Chen, E. Wijmans, S. Green, *et al.*, “The replica dataset: A digital replica of indoor spaces.” <https://arxiv.org/abs/1906.05797>, 2019.
- [3] A. Radford, J. W. Kim, C. Hallacy, A. Ramesh, G. Goh, S. Agarwal, *et al.*, “Learning transferable visual models from natural language supervision,” in *Proceedings of the 38th International Conference on Machine Learning*, vol. 139, pp. 8748–8763, PMLR, 2021.
- [4] A. Kirillov, E. Mintun, N. Ravi, H. Mao, C. Rolland, Gustafson, *et al.*, “Segment anything,” in *Proceedings of International Conference on Computer Vision*, 2023.
- [5] H. Liu, C. Li, Q. Wu, and Y. J. Lee, “Visual instruction tuning,” in *Proceedings of the Thirty-seventh Conference on Neural Information Processing Systems (NeurIPS)*, 2023.
- [6] OpenAI, “Gpt-4 technical report.” arXiv preprint arXiv:2303.08774, 2023.
- [7] Y. Hong, C. Lin, Y. Du, Z. Chen, J. B. Tenenbaum, and C. Gan, “3d concept learning and reasoning from multi-view images,” in *Proceedings of Computer Vision and Pattern Recognition*, 2023.
- [8] S. Peng, K. Genova, C. Jiang, A. Tagliasacchi, M. Pollefeys, and T. e. a. Funkhouser, “Openscene: 3d scene understanding with open vocabularies,” in *Proceedings of the IEEE/CVF Conference on Computer Vision and Pattern Recognition*, pp. 815–824, 2023.
- [9] Y. Hong, H. Zhen, P. Chen, S. Zheng, Y. Du, Z. Chen, and C. Gan, “3d-llm: Injecting the 3d world into large language models,” in *Neural Information Processing Systems*, 2023.
- [10] R. Ding, J. Yang, C. Xue, W. Zhang, S. Bai, and X. Qi, “Pla: Language-driven open vocabulary 3d scene understanding,” in *Proceedings of Computer Vision and Pattern Recognition*, 2023.
- [11] K. M. Jatavallabhula, A. Kuwajerwala, Q. Gu, M. Omama, G. Iyer, S. Saryazdi, *et al.*, “Conceptfusion: Open-set multimodal 3d mapping,” in *Robotics: Science and Systems*, 2023.
- [12] T. Luddecke and A. Ecker, “Image segmentation using text and image prompts,” in *2022 IEEE/CVF Conference on Computer Vision and Pattern Recognition (CVPR)*, June 2022.
- [13] T. Ren, S. Liu, A. Zeng, J. Lin, K. Li, H. Cao, *et al.*, “Grounded sam: Assembling open-world models for diverse visual tasks.” <http://arxiv.org/abs/2401.14159>, Jan. 2024.
- [14] J. Li, D. Li, C. Xiong, and S. Hoi, “Blip: Bootstrapping language-image pre-training for unified vision-language understanding and generation,” in *Proceedings of the 39th International Conference on Machine Learning*, vol. 162, PMLR, 2022.
- [15] B. Li, K. Q. Weinberger, S. Belongie, V. Koltun, and R. Ranftl, “Language-driven semantic segmentation,” in *International Conference on Learning Representations (ICLR)*, 2022.
- [16] F. Liang, B. Wu, X. Dai, K. Li, Y. Zhao, H. Zhang, *et al.*, “Open-vocabulary semantic segmentation with mask-adapted clip,” in *Conference on Computer Vision and Pattern Recognition (CVPR)*, 2023.
- [17] X. Zou, J. Yang, H. Zhang, F. Li, L. Li, J. Wang, *et al.*, “Segment everything everywhere all at once.” <http://arxiv.org/abs/2304.06718>, 2023.
- [18] T. B. Brown, B. Mann, N. Ryder, M. Subbiah, J. Kaplan, P. Dhariwal, *et al.*, “Language models are few-shot learners,” *ArXiv*, vol. abs/2005.14165, 2020.
- [19] H. Touvron, T. Lavril, G. Izacard, X. Martinet, M.-A. Lachaux, T. Lacroix, *et al.*, “Llama: Open and efficient foundation language models,” *ArXiv*, vol. abs/2302.13971, 2023.
- [20] H. Liu, C. Li, Y. Li, and Y. J. Lee, “Improved baselines with visual instruction tuning.” <http://arxiv.org/abs/2310.03744>, Oct. 2023.
- [21] M. Grinvald, F. Furrer, T. Novkovic, J. J. Chung, C. Cadena, R. Siegwart, and J. Nieto, “Volumetric instance-aware semantic mapping and 3d object discovery,” *IEEE Robotics and Automation Letters*, 2019.
- [22] A. Rosinol, M. Abate, Y. Chang, and L. Carlone, “Kimera: An open-source library for real-time metric-semantic localization and mapping,” in *ICRA*, 2020.
- [23] N. Hughes, Y. Chang, and L. Carlone, “Hydra: A real-time spatial perception system for 3D scene graph construction and optimization,” in *Robotics: Science and Systems (RSS)*, 2022.
- [24] S.-C. Wu, J. Wald, K. Tateno, N. Navab, and F. Tombari, “Scenegrph-fusion: Incremental 3d scene graph prediction from rgb-d sequences,” in *Proceedings of the IEEE/CVF Conference on Computer Vision and Pattern Recognition*, pp. 7515–7525, 2021.
- [25] S.-C. Wu, K. Tateno, N. Navab, and F. Tombari, “Incremental 3d semantic scene graph prediction from rgb sequences,” in *Proceedings of the IEEE/CVF Conference on Computer Vision and Pattern Recognition*, 2023.
- [26] Y. Yang, X. Wu, T. He, H. Zhao, and X. Liu, “Sam3d: Segment anything in 3d scenes.” <https://arxiv.org/abs/2306.03908v1>, 2023.
- [27] A. Takmaz, E. Fedele, R. Sumner, M. Pollefeys, F. Tombari, and F. Engelmann, “Openmask3d: Open-vocabulary 3d instance segmentation,” in *Advances in Neural Information Processing Systems (A. Oh, T. Neumann, A. Globerson, K. Saenko, M. Hardt, and S. Levine, eds.)*, vol. 36, pp. 68367–68390, Curran Associates, Inc., 2023.
- [28] J. Schult, F. Engelmann, A. Hermans, O. Litany, S. Tang, and B. Leibe, “Mask3d: Mask transformer for 3d semantic instance segmentation,” in *International Conference on Robotics and Automation (ICRA)*, 2023.
- [29] J. Yang, X. Chen, S. Qian, N. Madaan, M. Iyengar, D. F. Fouhey, and J. Chai, “Llm-grounder: Open-vocabulary 3d visual grounding with large language model as an agent,” 2023.
- [30] J. Yang, H. Zhang, F. Li, X. Zou, C. Li, and J. Gao, “Set-of-mark prompting unleashes extraordinary visual grounding in gpt-4v,” 2023.
- [31] R. Huang, S. Peng, A. Takmaz, F. Tombari, M. Pollefeys, S. Song, G. Huang, and F. Engelmann, “Segment3d: Learning fine-grained class-agnostic 3d segmentation without manual labels,” 2023.
- [32] Z. Huang, X. Wu, X. Chen, H. Zhao, L. Zhu, and J. Lasenby, “Openins3d: Snap and lookup for 3d open-vocabulary instance segmentation,” *arXiv preprint*, 2023.
- [33] K. Rana, J. Haviland, S. Garg, J. Abou-Chakra, I. Reid, and N. Suennderhauf, “Sayplan: Grounding large language models using 3d scene graphs for scalable task planning,” in *7th Annual Conference on Robot Learning*, 2023.
- [34] Q. Gu, A. Kuwajerwala, S. Morin, K. M. Jatavallabhula, B. Sen, A. Agarwal, *et al.*, “Conceptgraphs: Open-vocabulary 3d scene graphs for perception and planning,” 2023.
- [35] Y. Zhang, X. Huang, J. Ma, Z. Li, Z. Luo, Y. Xie, *et al.*, “Recognize anything: A strong image tagging model.” <http://arxiv.org/abs/2306.03514>, Feb. 2024.
- [36] S. Liu, Z. Zeng, T. Ren, F. Li, H. Zhang, J. Yang, *et al.*, “Grounding dino: Marrying dino with grounded pre-training for open-set object detection.” arXiv preprint arXiv:2303.05499, 2023.